Factors Influencing the Efficacy of Forward-Looking Infrared in Polar Bear Den Detection

Article *in* BioScience · July 2014

1 author:

Rusty Robinson
Brigham Young University - Provo Main Campus
3 PUBLICATIONS **4** CITATIONS

SEE PROFILE

Factors Influencing the Efficacy of Forward-Looking Infrared in Polar Bear Den Detection

RUSTY ROBINSON, TOM S. SMITH, RANDY T. LARSEN, AND BJ KIRSCHHOFFER

Female polar bears construct maternal dens in snowdrifts in autumn. Forward-looking infrared (FLIR) has been used to locate dens to prevent disruption of denning by human activities, but the results have been mixed. To identify limitations and optimal conditions for locating dens, we took handheld FLIR images of three artificial dens under varied conditions. We tested variables hypothesized to influence detectability with linear models using the zero-inflated negative binomial distribution. Solar radiation, wind speed, and den wall thickness reduced the likelihood of detecting dens. The negative effect of wind speed on detectability increased with increasing distance. To maximize the efficacy of ground-based FLIR, den surveys should be conducted when solar radiation is less than 16 watts per square meter (night) and when wind speed is less than 10 kilometers per hour. Adherence to these guidelines will maximize the protection that FLIR can afford to denning bears.

Keywords: Alaska, handheld FLIR, maternal den, polar bear, Ursus maritimus

Pregnant polar bears in the southern Beaufort Sea and the adjoining coastal areas use dens from October through November (Amstrup and Gardner 1994). Cubs are born in midwinter and remain at the den until March or April (Blix and Lentfer 1979, Amstrup 1993, Amstrup and Gardner 1994, Smith et al. 2007). A disturbance while den sites are active may have greater negative effects on survival and reproduction than one at any other time of year (Linnell et al. 2000). Disturbance may result in displacement, exposure to the elements and predation, family dissolution, and cub abandonment and subsequent death. Consequently, the ability of scientists to identify den sites is key to limiting negative influences from disturbance.

Expanding petroleum exploration along Alaska's North Slope area coupled with a shift to terrestrial dens (Amstrup and Gardner 1994, Fischbach et al. 2007) heightens the likelihood of bear–human interactions. Furthermore, industry can be required to limit or cease activities in the vicinity of known dens or can be fined for den disturbance by the US Fish and Wildlife Service, the regulatory agency tasked with managing polar bears. Consequently, much work has been done to identify and map suitable denning habitat in order to avoid potential conflicts with and to mitigate the disturbance of polar bears (Amstrup 1993, Durner et al. 2001, 2003, Blank 2012). Denning habitat occurs in areas such as riverbanks and coastal bluffs, where drifting snow accumulates (Amstrup 1993, Amstrup and Gardner 1994, Durner et al. 2001, 2003). Forward-looking infrared (FLIR) has been used to survey denning habitat and locate dens prior to constructing ice roads and other production efforts (Amstrup et al. 2004).

FLIR imagers can be mounted on vehicles (e.g., aircraft, trucks, track vehicles) or can be handheld; these platforms have proven to be useful for identifying and locating polar bear dens. FLIR imagers are capable of detecting the very slight temperature differences (changes as small as 0.01 degree Celsius [°C]) on the surface of a snow bank resulting from denned polar bears (Amstrup et al. 2004). Temperature differences are shown in the imager's display as varying shades of color, with lighter colors representing warmer temperatures. In the FLIR imager, polar bear dens generally appear as light-colored hot spots, with soft edges that gradate into the surrounding darker, colder terrain (see figure 2 in Amstrup et al. 2004). To optimize den detectability with handheld FLIR, it is important to identify factors that influence the image quality. Although atmospheric conditions (i.e., relative humidity, temperature, dew point, precipitation, wind) have been known to influence the effectiveness of aerial FLIR when they are used for den detection, the critical thresholds for detection have not been identified (Amstrup et al. 2004). The purpose of the present study is to model the variables that influence the ability of handheld FLIR to detect dens and to identify the optimal conditions for conducting polar bear den surveys with handheld FLIR.

BioScience 64: 735–742.
doi:10.1093/biosci/biu095 Advance Access publication 16 July 2014

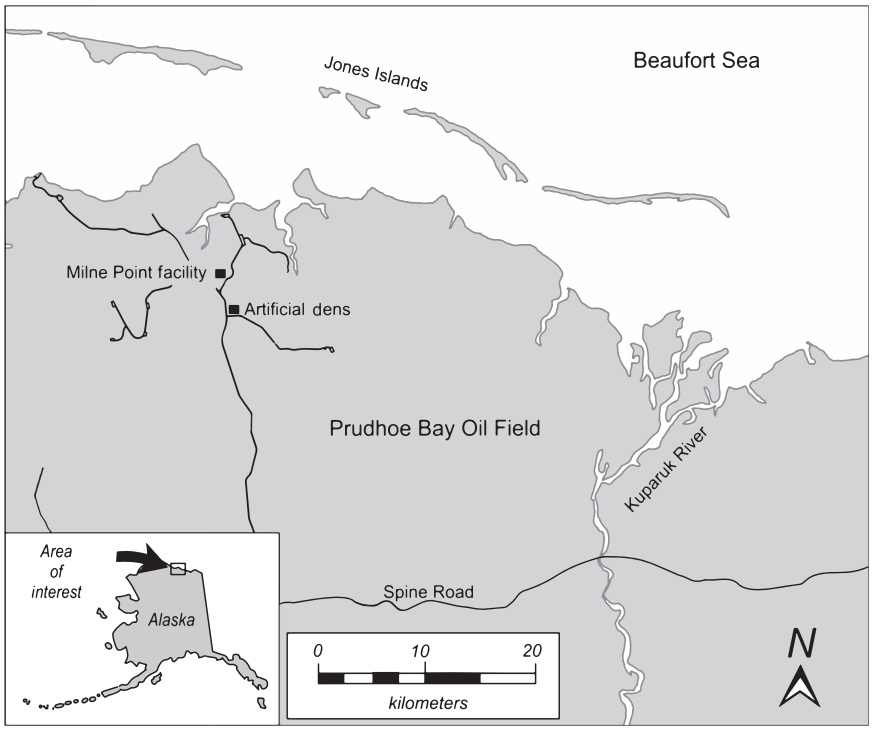

Figure 1. Study area south of Milne Point, Alaska, where artificial den forward-looking infrared sampling took place in March 2010.

The study area was located west of Prudhoe Bay, Alaska, in the Prudhoe Bay oil field. This area is composed largely of BP (formerly British Petroleum) lease lands that have been developed for oil exploration and production, including scattered gravel pads and industrial facilities, linked by 4800 kilometers (km) of pipeline and roads. Our study took place approximately 1.6 km south of the BP Milne Point processing facility (70.4587 degrees north, 149.4414 degrees west; figure 1). For the construction of artificial dens for this study, we selected a snowdrift approximately 60 meters (m) long and 4 m high. The artificial dens were excavated approximately 20 m from a small, unheated structure that provided electricity for den heaters.

Excavating dens

In February 2010, we excavated three artificial polar bear dens with initial snow wall thicknesses of 25, 50, and 75 centimeters (cm) in a south-facing snowdrift. To construct these dens, we excavated from the top of the drift down 2 m using snow shovels and snow saws. The initial dimensions of each den were approximately 1 × 1 × 2 m (figure 2). The dens were excavated 3 m apart (from edge to edge). We placed a 200-watt ceramic heater in each den, simulating the heat generated by a denning polar bear (Watts 1983). We used measuring sticks to monitor changes in den wall thickness throughout the sampling period as snow depth changed because of wind and snowfall. Each measuring stick had a stopper on the end inside the den that we pulled tight against the inner wall after the dens had melted to a stable size and before any sampling began. For the duration of the study, the den chamber access shafts were sealed with plywood lids over which snow was backfilled for insulation. After turning the heaters on, we allowed the den temperatures to stabilize for 2 weeks (a conservative time frame based on previous trials that we had performed) prior to sampling. We began sampling den heat loss with FLIR on 11 March 2010. After the study was concluded, we opened the dens and ensured that the stoppers were still against the inner wall and that the wall thickness measurements were accurate.

Den sampling

Using a FLIR ThermaCAM P65HS thermal imager (FLIR Systems, Boston, Massachusetts) with a 72 millimeter infrared lens, we sampled one or more times daily (mean [*M*] = 3). Sampling was scheduled at stratified intervals with consideration of *solar time*, the time relative to the sun's position in the sky, thus was the variation in solar radiation accounted for (figure 3). During each sample period, we recorded images from three distances: 60 m, the minimum distance that the US Fish and Wildlife Service allowed (through permit MA225854) for handheld FLIR surveys for polar bear dens; 100 m; and 200 m. A laser rangefinder was used to determine the distance. To ensure accurate thermal readings, we entered the required parameters into the imager settings, including the air temperature, the relative humidity, the distance, the emissivity, and the reflected temperature, before each sampling period. Excluding these parameters does not affect the visual appearance of the image that is saved to the imager but does affect the accuracy of specific pixel temperatures used in later analysis. The air temperature and relative humidity were determined using a Kestrel 3000 weather meter (Nielsen-Kellerman, Birmingham, Michigan). *Emissivity*, a measure of a substance's ability to release thermal energy, was set to .85 for snow, as was specified by the manufacturer of the FLIR device. The reflected temperature was calculated according to the FLIR manual instructions by facing the FLIR imager in the opposite direction of the snowdrift, setting the emissivity to 1, adjusting to near focus, saving an image, and using the box function to calculate an average temperature. In addition to air temperature and relative humidity, we recorded the wind speed and the temperature–dew point spread (the dew point subtracted from the air temperature) with the same weather meter, placed at the 100-m sampling location at the same height as the FLIR imager. The presence of precipitation was noted, and the solar radiation data were provided by a research weather

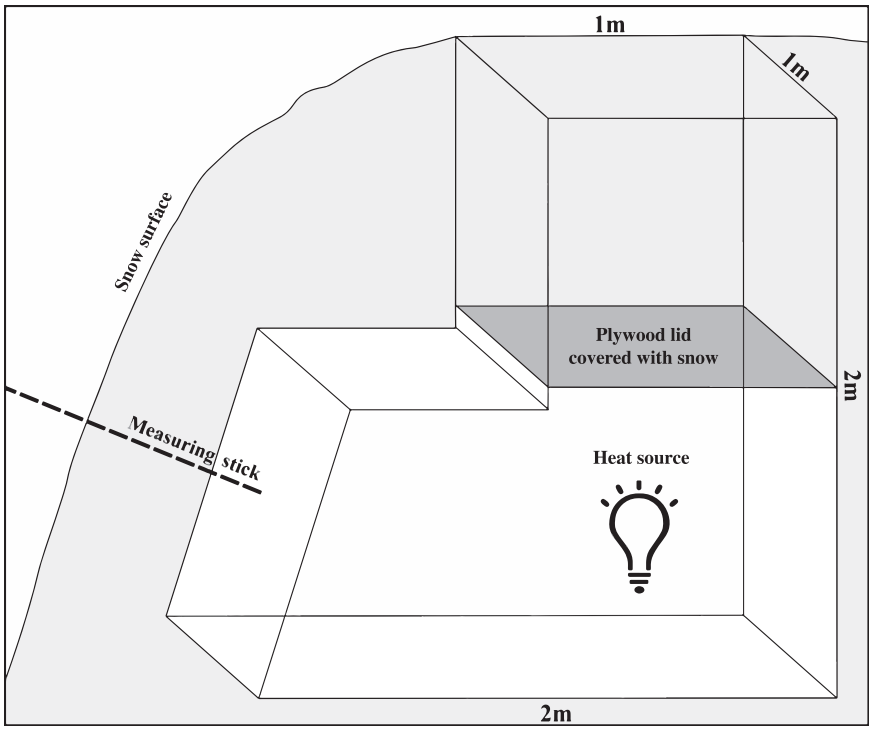

Figure 2. Artificial snow den structure used to test the efficacy of handheld forward-looking infrared for detecting polar bear maternal dens. The shaded area represents snow cover. Abbreviation: m, meters.

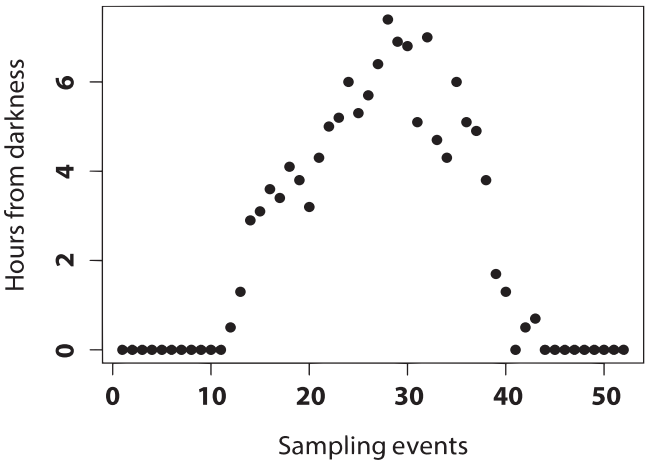

Figure 3. Sampling time distribution in relation to solar time used in forward-looking infrared sampling of artificial dens.

station at BP's F-Pad facility, 11 km from the study site, after the handheld sensor that we were using had failed. The solar sensors at the weather station were oriented horizontally, not perpendicular to the frontal slope of the artificial dens, but still gave consistent and reliable readings relative to the solar radiation received at the den sites. Resting the imager on posts marking each sample distance, we recorded images at each distance. The den wall thickness was recorded by walking along the top of the snowdrift and peering over the side of the drift to view the measuring stick protruding from each den. These measurements were taken directly after the conclusion of each sampling event to ensure that the thermal properties of the dens were not disturbed before or during sampling. We never walked on or otherwise disturbed the surface of the drift being sampled.

After data collection, we downloaded the images and assigned each a detectability score. We first determined whether a hot spot was detectable to the human eye in each sample image. If it was not, the image was automatically given a detectability score of 0. If a hot spot was visible, we calculated the detectability score using FLIR Quick Report (FLIR Systems), a software package used to organize and analyze thermal images taken with FLIR cameras. The software features an area tool that highlights an area of interest and exports temperature data for each pixel. We created a rectangle that encompassed a typical hot spot at each distance (26 × 41 pixels for 60 m, 21 × 28 for 100 m, 12 × 16 for 200 m). This rectangle was centered over each hot spot and the pixel temperatures were exported for the next step of the analysis. The mean background temperature of the surrounding snowdrift was determined in the same manner. To determine a detectability score for each hot spot, we subtracted the mean background temperature of the snowdrift from the temperature of each pixel within the hot spot to calculate the total change in temperature for all of the pixels within the hot spot, thus generating a sum total temperature above background for each den image (i.e., the detectability score).

Statistical analysis

We were unable to identify the den's hot spot (i.e., the detectability score was 0) in many images. As a result, we used linear models with the zero-inflated negative binomial distribution for the error structure in our modeling. Advances with linear models that use zero-inflated distributions (e.g., zero-inflated negative binomial or zero-inflated Poisson distribution) provide a solution to count data with excess zeroes (Lambert 1992, Welsh et al. 1996). With these models, one can evaluate the influence of explanatory variables on both the count response and the probability of a zero count. Zero-inflated models estimate a point mass at zero in addition to standard distributional estimates and have been successfully used with ecological data in a variety of settings (Welsh et al. 1996, Martin et al. 2005, Arab et al. 2008). These methods

Table 1a. Supported models ($W_i > 0.01$) for the detectability (count) analysis, artificial den forward-looking infrared sampling at Prudhoe Bay, Alaska, March 2010.

Model number	Variables	AICc	ΔAICc	W_i
26	Precipitation, solar radiation, wind speed	468.65	0.00	0.74
28	Solar radiation, den wall thickness, wind speed	471.14	2.49	0.21
16	Precipitation, solar radiation	475.37	6.72	0.03
32	Precipitation, solar radiation, temperature–dew point spread	476.81	8.16	0.01

Abbreviations: AICc, Akaike's information criterion adjusted for a small sample size; ΔAICc, the change in the AICc value compared with the top model; W_i, the AICc weight.

Table 1b. Supported models ($W_i > 0.01$) for the distance analysis, artificial den forward-looking infrared sampling at Prudhoe Bay, Alaska, March 2010.

Model number	Variables	AICc	ΔAICc	W_i
9	Precipitation, wind speed	794.80	0.00	0.15
1	Wind speed	794.86	0.06	0.15
10	Humidity, wind speed	795.59	0.79	0.10
8	Solar radiation, wind speed	796.42	1.61	0.07
23	Precipitation, temperature–dew point spread, wind speed	796.42	1.62	0.07
29	Humidity, precipitation, wind speed	796.61	1.8	0.06
11	Den wall thickness, wind speed	796.81	2.01	0.06
30	Precipitation, den wall thickness, wind speed	796.85	2.04	0.06
7	Temperature–dew point spread, wind speed	796.97	2.16	0.05
26	Precipitation, solar radiation, wind speed	796.98	2.17	0.05
24	Humidity, temperature–dew point spread, wind speed	797.55	2.75	0.04
31	Humidity, den wall thickness, wind speed	797.62	2.82	0.04
27	Humidity, solar radiation, wind speed	797.75	2.94	0.04
22	Solar radiation, temperature–dew point spread, wind speed	798.35	3.55	0.03
28	Solar radiation, den wall thickness, wind speed	798.42	3.61	0.03
25	Temperature–dew point spread, den wall thickness, wind speed	798.95	4.15	0.02

Abbreviations: AICc, Akaike's information criterion adjusted for a small sample size; ΔAICc, the change in the AICc value compared with the top model; W_i, the AICc weight.

reduce bias in the parameter estimates associated with large numbers of zeroes.

To assess the influence of factors on detectability, we used an information-theoretic approach, Akaike's information criterion, adjusted for small sample size, to rank the models (Akaike 1973, Burnham and Anderson 2002). We constructed 40 models in total (table 1a and 1b) by including permutations of the six variables of interest (solar radiation, wind speed, den wall thickness, relative humidity, temperature–dew point spread, and the presence of precipitation) while excluding models with more than three variables (the maximum allowable number of parameters) and one model with a convergence error. We then averaged over all of the models for each den using the MuMin package (*http://cran.r-project.org/web/packages/MuMIn/index.html*) and the glmmADMB package (*http://glmmadmb.r-forge.r-project.org*) in the R programming language (version 2.10.0, R Foundation for Statistical Computing, Vienna, Austria) to evaluate the direction and strength of associations between the explanatory variables and den detectability. We also used the pscl (*http://pscl.stanford.edu*), calibrate (*http://CRAN.R-project.org/package=calibrate*), and MASS (*http://cran.r-project.org/web/packages/MASS/index.html*) packages in R to perform the analyses. This modeling was performed only with the 100-m data. The images taken from 60 and 200 m were used to analyze the effects of each variable as distance increased.

As the sampling distance changed, variation in the detectability coefficients largely became a function of the number of pixels within the standardized area-tool rectangle used for each distance instead of actual trends. As a result, it became necessary to exclude distance as a variable of interest in our modeling approach and to analyze it separately. The same models and methods were used for this analysis (table 1b), but it included only den images that contained hot spots visible to the human eye ($n = 102$), so we did not

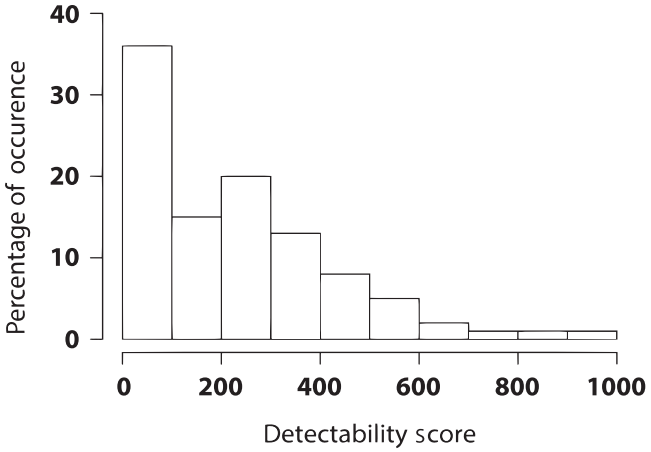

Figure 4. Detectability scores from the forward-looking infrared imaging samples at a 100-meter distance.

include a zero-inflated portion in this modeling approach. Forty-one models were included in this analysis. As the distance increased between an artificial den and the FLIR imager, the atmospheric effects also increased. To account for this in our analysis, we compared declines in the actual detectability score with the score declines that would be expected without atmospheric effects. Because an image taken at 200 m contains only 30% of the pixels that are contained in a 60 m image (60 ÷ 200), the detectability score at 200 m would be 30% of the 60 m score. To determine the relative influence of atmospheric conditions, we calculated the percentage of actual score decline compared with the predicted score decline without atmospheric influence by dividing the actual score decline (200 m score ÷ 60 m score) by the predicted score decline (0.30). Therefore, a lower percentage would theoretically signify a greater effect of atmospheric conditions on the detectability of the hot spot. We averaged over all of the models and assessed each variable for significance ($\alpha = .05$). We also analyzed the effect of den wall thickness on detectability by regressing the detectability scores and the den wall thickness to estimate the thresholds of detection.

Modeling of covariates

Over a period of 19 days, we conducted 52 sampling sessions. All three dens were measured during each sampling period. The detectability scores ranged from 0 to 927, although 33% of the sample images yielded a detectability score of 0. The resulting frequency histograms of detectability scores were typical of those associated with zero-inflated data (figure 4). The solar radiation ranged from 0 to 320.3 watts per square meter (W/m^2), the wind speed ranged from 2.4 to 32.5 km per hour, precipitation was present during 19 sampling events, the relative humidity ranged from 68.8% to 86.2%, the den wall thickness ranged from 30 to 80 cm, and the temperature–dew point spread ranged from 0.5°C to 9.3°C during the sampling period.

After reopening the dens at the conclusion of the study, we found that all three dens had melted out to similar volume approximations (M = 3.32 m^3, standard deviation [SD] = 0.14) because of heater effects and were within the range of natural den chambers previously reported in the southern Beaufort Sea and eastern Canada (Harington 1968, Durner et al. 2003). In addition, we noted that a 2.5-cm-thick ice lens had formed on the inner surface of each chamber, which also occurs in actual polar bear dens (Harrington 1968, Durner et al. 2003).

The best-fit model for detectability was the same for each den and included solar radiation, wind speed, and the presence of precipitation (table 1a). Wind speed was negatively correlated ($p < .01$) with detectability. Solar radiation was negatively correlated with detectability in den 1 ($p < .01$) but not in dens 2 and 3. The den wall thickness was negatively correlated with detectability in den 3 ($p < .05$) but not significantly in dens 1 and 2. The temperature–dew point spread and relative humidity were positively correlated with detectability, but only the temperature–dew point spread correlation was significant ($p < .05$) and only in den 1. In the zero-inflated portion of this model, wind speed, solar radiation, den wall thickness, and temperature–dew point spread were positively correlated with the probability of a 0 score. However, the only variables for which there was a significant effect were solar radiation ($p < .01$) in all three dens and den wall thickness ($p < .05$) in dens 1 and 3. Thickness was strongly correlated with detectability in den 2 ($p < .1$). Humidity and the presence of precipitation were negatively correlated with the probability of obtaining a zero score, neither of which was significant.

After averaging the coefficients of all three den analyses, we found that there were significant effects for solar radiation, wind speed, and den wall thickness (table 2). Solar radiation negatively affected the detectability scores for the count portion of the models (figure 5), with a 1-W/m^2 increase in solar radiation decreasing detection by a factor of 0.998 ($p < .05$). In the zero-inflated portion of the models, solar radiation was positively correlated with obtaining a 0 score, with a 1-W/m^2 increase in solar radiation increasing the odds of a den receiving a 0 score (i.e., of not being detected) by a factor of 1.027 ($p < .01$). Wind speed was negatively correlated with detectability in the count portion of the model (figure 6), with a 1-km-per-hour increase in wind speed decreasing den detection by a factor of 0.954 ($p < .01$). Den wall thickness was positively correlated with the probability of a 0 score. A 1-cm increase in den wall thickness increased the odds of a den receiving a 0 score by a factor of 1.485 ($p < .05$). We found the mean point of den wall thickness at which the dens became undetectable to be 90 cm.

For the distance portion of the analysis, the best-fit model included wind speed and precipitation. Wind speed was the only variable that was significant (figure 7). It was negatively correlated with detectability and was included in all

Table 2. Model-averaged coefficients with associated p*-values from forward-looking infrared sampling of artificial polar bear dens at Prudhoe Bay, Alaska, March 2010.*

	Count				Zero-inflation			
Variable	Estimate	Standard error	*z*	*p*	Estimate	Standard error	*z*	*p*
Intercept	6.54	0.57	17.54	$<2e^{-16}$	–6.61	9.27	0.97	.37
Wind speed	–0.05	0.01	3.98	<.01	0.04	0.12	0.37	.71
Solar radiation	$-1.86e^{-03}$	0.00	2.10	<.05	0.03	0.01	3.08	<.01
Precipitation	–0.16	0.19	0.77	.47	–22.61	5045.00	$4.33e^{-03}$	1.00
Temperature–dew point spread	0.09	0.05	1.78	.08	0.01	0.49	0.22	.83
Humidity	0.85	2.82	0.30	.76	–22.28	21.07	1.01	.35
Den wall thickness	–0.04	0.03	1.30	.30	0.36	0.17	2.03	<.05

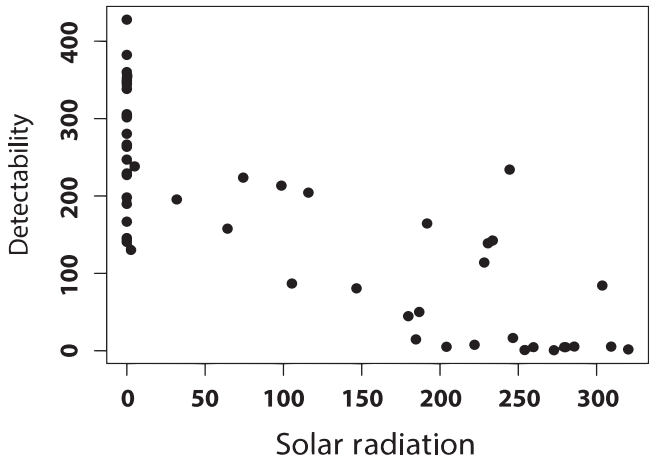

Figure 5. The relationship between solar radiation (in watts per square meter) and den detectability for all three dens at a 100-meter distance.

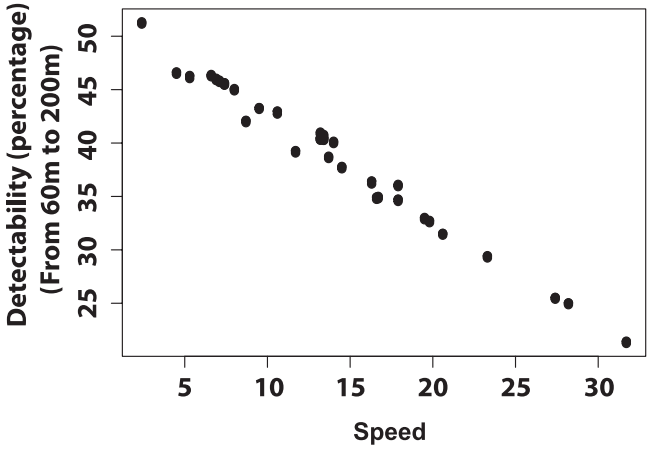

Figure 7. The relationship between wind speed (in kilometers per hour) and den detectability as distance increased.

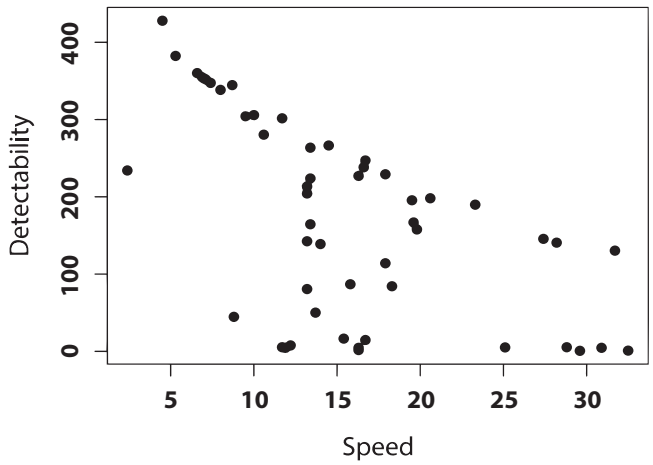

Figure 6. The relationship between wind speed (in kilometers per hour) and den detectability for all three dens at a 100-meter distance.

16 supported models (table 1b; greater than 99% weight). A 1-km-per-hour increase in wind speed increased the spread between the predicted and the actual detectability by a factor of 0.404 ($p < .01$).

Conclusions

Amstrup and colleagues (2004) identified solar radiation, airborne moisture, and temperature–dew point spread as important factors in polar bear den detection using aircraft-based FLIR. Our findings are similar with regard to both solar radiation and temperature–dew point spread, although we did not use airborne moisture as a metric. Rather, we used precipitation (falling or suspended moisture) as one metric and wind speed, which accounts for blowing snow, as another. We did not find precipitation alone to have a significant effect in any of our models. However, only light precipitation occurred during our sampling sessions, which probably limited our ability to evaluate its influence. Poor FLIR performance has been observed during moderate snowfall in the attempted detection of

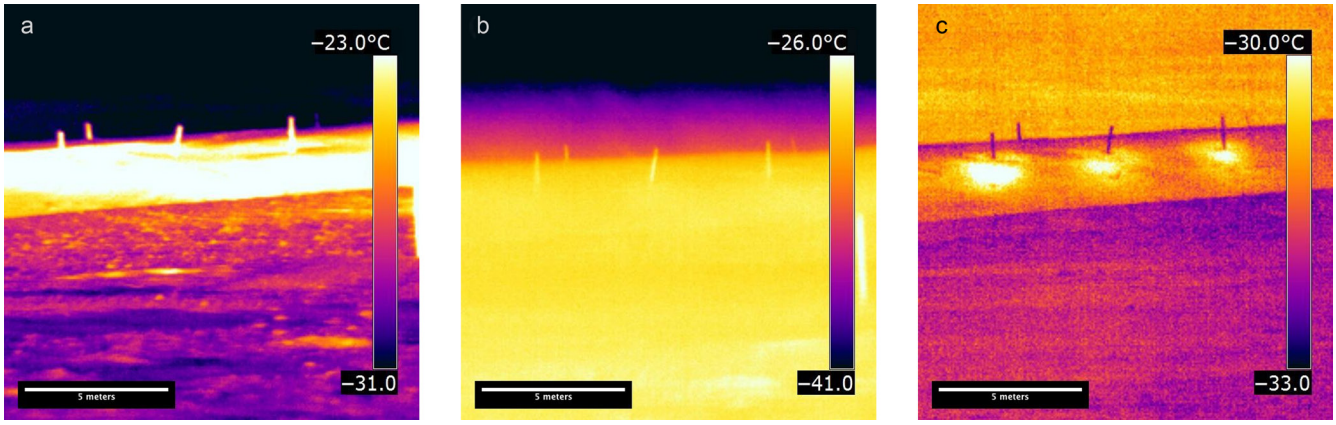

Figure 8. Infrared images of artificial dens at a 100-meter distance showing (a) sunny conditions, (b) windy conditions, and (c) optimal conditions. Abbreviation: °C, degrees Celsius. Photographs: Rusty Robinson.

actual polar bear dens (Smith et al. 2007). Therefore, precipitation and its intensity should also be considered (Amstrup et al. 2004).

Solar radiation and wind speed were the most important factors influencing artificial polar bear den detection using FLIR (figures 8–10). Of the den images in which the dens were not detectable (n = 47), 94% had solar radiation greater than 100 W/m^2. Conversely, only 39% of detectable den images (n = 109) had solar radiation greater than 0 W/m^2. Regardless of all other variables, 96% of the dens sampled at night (n = 69) were detectable at some level. Den detectability scores were 2.7 times higher in hours of darkness than when sunlight was present. Because of convection and blowing ground snow (i.e., wind-driven snow close to the ground), wind had a negative effect on den detectability in general and as horizontal distance to the den increased in particular. However, detectability as vertical distance increases may not be affected by wind as much as it is with horizontal increases. Imagers on the ground are subject to compounding ground snow particles as distance increases, whereas an aircraft-based imager may be subject only to the blowing snow directly over the den. Even if this is the case, convection and the constantly moving particles will still have a negative effect on detection, and we recommend that windy conditions be avoided altogether, regardless of the imaging platform.

Ice lens formation on the inner surfaces of natural polar bear dens has been reported (Harington 1968, Durner et al. 2003), but polar bears will usually scrape at the walls and ceilings with their claws, leaving little if any ice. The influence of ice on den detectability was not tested, but, because den wall thickness had a significant effect in the zero-inflated portion of our modeling, it is possible that ice also has an effect on detectability. This could result in a difference in heat dissipation relative to natural dens. In spite of this concern, we think that our artificial dens simulated real dens adequately to evaluate useful detection methods. Specific thresholds may need further testing.

The snow depth above the chamber of a polar bear den can vary greatly (M = 72 cm, SD = 87) and has been measured up to 400 cm (Durner et al. 2003). This suggests that a large portion of dens have wall thicknesses greater than 90 cm and would probably go undetected regardless of survey conditions. During the course of this study, den wall thickness fluctuated as much as 16 cm with changing wind, and a single windstorm before the study began added 4 horizontal meters and 2 vertical meters of snow to our sample snowdrift. We recommend conducting FLIR surveys as early as possible in the denning period, when the snow depth over dens is expected to be at winter minimums (Uspenski and Kitchinski 1972).

In order to reach maximum detectability (in the top 10% for each den at 100 m), we recommend that managers tasked with locating polar bear dens using handheld FLIR do so between dusk and dawn when the wind is slower than 10 km per hour. The mean solar radiation for the top 10% of the detectability scores was 16 W/m^2, with all but one top score occurring at night. If surveys must be conducted during daylight hours, time periods near dawn or dusk with heavy cloud cover should be sought in order to minimize the effects of solar radiation. Although all of our measurements were collected on the ground, they largely corroborate past work (Amstrup et al. 2004) and our observations with aerial FLIR. Our findings here probably apply to aerial FLIR, as well. We think that by following these recommendations, polar bear den detection will be optimized, thus will potential negative impacts associated with the interactions of denning polar bears and industry be avoided.

Acknowledgments

We thank Neil Hermon, Rob Murray, Deb Heebner, Karen Ford-Thomas, Fire Chief John Rychlinski, security personnel, and all our other friends at Milne Point for always being helpful and supportive. Bill Streever, Diane Sanzone, and Tatyana Swanson, with BP, were instrumental in getting this project off the ground, and we appreciate their tireless efforts.

We are deeply indebted to Robert and Carolyn Buchanan, as well as the entire Polar Bears International family, for their continued support and hard work. Thanks to Michael Lilly and David Shahon, who donated their time and expertise to the project. We sincerely appreciate Steve Amstrup, Anthony Fischbach, and anonymous reviewers for their valuable input.

References cited

Akaike H. 1973. Information theory and an extension of the maximum likelihood principle. Pages 267–281 in Petrov BN, Caski F, eds. Proceedings of the Second International Symposium on Information Theory. Akademiai Kiado.

Amstrup SC. 1993. Human disturbances of denning polar bears in Alaska. Arctic 46: 246–250.

Amstrup SC, Gardner C. 1994. Polar bear maternity denning in the Beaufort Sea. Journal of Wildlife Management 58: 1–10.

Amstrup SC, York G, McDonald TL, Nielson R, Simac K. 2004. Detecting denning polar bears with forward-looking infrared (FLIR) imagery. BioScience 54: 337–344.

Arab A, Wildhaber ML, Wikle CK, Gentry CN. 2008. Zero-inflated modeling of fish catch per unit area resulting from multiple gears: Application to channel catfish and shovelnose sturgeon in the Missouri River. North American Journal of Fisheries Management 28: 1044–1058.

Blank JJ. 2012. Remote Identification of Maternal Polar Bear (*Ursus maritimus*) Denning Habitat on the Colville River Delta, Alaska. Master's thesis. University of Alaska, Anchorage.

Blix AS, Lentfer JW. 1979. Modes of thermal protection in polar bear cubs—At birth and on emergence from the den. American Journal of Physiology 236: R67–R74.

Burnham KP, Anderson DR. 2002. Model Selection and Multimodel Inference: A Practical Information-Theoretic Approach, 2nd ed. Springer.

Durner GM, Amstrup SC, Ambrosius KJ. 2001. Remote identification of polar bear maternal den habitat in northern Alaska. Arctic 54: 115–121.

Durner GM, Amstrup SC, Fischbach AS. 2003. Habitat characteristics of polar bear terrestrial maternal den sites in northern Alaska. Arctic 56: 55–62.

Fischbach AS, Amstrup SC, Douglas DC. 2007. Landward and eastward shift of Alaskan polar bear denning associated with recent sea ice changes. Polar Biology 30: 1395–1405.

Harington CR. 1968. Denning habits of the polar bear (*Ursus maritimus* Phipps). Canadian Wildlife Service. Report no. 5.

Lambert D. 1992. Zero-inflated Poisson regression, with an application to defects in manufacturing. Technometrics 34: 1–14.

Linnell JDC, Swenson JE, Andersen R, Barnes B. 2000. How vulnerable are denning bears to disturbance? Wildlife Society Bulletin 28: 400–413.

Martin TG, Wintle BA, Rhodes JR, Kuhnert PM, Field SA, Low-Choy SJ, Tyre AJ, Possingham HP. 2005. Zero tolerance ecology: Improving ecological inference by modelling the source of zero observations. Ecology Letters 8: 1235–1246.

Smith TS, Partridge ST, Amstrup SC, Schliebe S. 2007. Post-den emergence behavior of polar bears (*Ursus maritimus*) in northern Alaska. Arctic 60: 187–194.

Uspenski SM, Kitchinski AA. 1972. New data on the winter ecology of the polar bear (*Ursus maritimus* Phipps) on Wrangel Island. Pages 181–197 in Herrero S, ed. Bears: Their Biology and Management, vol. 2. International Association for Bear Research and Management.

Watts P. 1983. Ecological Energetics of Denning Polar Bears and Related Species. PhD dissertation, University of Oslo, Norway.

Welsh AH, Cunningham RB, Donnelly CF, Lindenmayer DB. 1996. Modelling the abundance of rare species: Statistical models for counts with extra zeros. Ecological Modelling 88: 297–308.

Rusty Robinson (rustyrobinson@byu.net) is a master's candidate, Tom S. Smith is an associate professor, and Randy T. Larsen is an assistant professor at Brigham Young University, in Provo, Utah. BJ Kirschhoffer is the director of field operations at Polar Bears International, in Bozeman, Montana.